Inverse design of compounds that have simultaneously ferroelectric and Rashba cofunctionality

Carlos Mera Acosta [1,2,*] Adalberto Fazzio,[3] Gustavo M. Dalpian,[2] and Alex Zunger [1,†]

[1] ⬝⬝⬝⬝⬝⬝⬝⬝⬝⬝⬝⬝⬝⬝⬝⬝⬝⬝⬝⬝⬝⬝⬝⬝⬝⬝⬝⬝⬝⬝⬝⬝⬝⬝⬝

[2] ⬝⬝⬝⬝⬝⬝⬝⬝⬝⬝⬝⬝⬝⬝⬝⬝⬝⬝⬝⬝⬝⬝⬝⬝⬝⬝⬝⬝⬝⬝⬝⬝⬝⬝

[3] ⬝⬝⬝⬝⬝⬝⬝⬝⬝⬝⬝⬝⬝⬝⬝⬝⬝⬝⬝⬝⬝⬝⬝⬝⬝⬝⬝⬝⬝⬝⬝⬝⬝⬝

Cofunctionality—the coexistence of different (possibly even contraindicated) proper⬝⬝⬝⬝⬝⬝⬝⬝⬝⬝⬝⬝⬝⬝⬝⬝⬝⬝⬝⬝⬝⬝⬝⬝⬝⬝⬝⬝⬝⬝

(2D) materials [10,11], topological insulators [12–14], and ferroelectric materials [15–17]. The data obtained from such direct calculations or measurements can also be used in machine learning, thereby providing an interpolation formula (in terms of phenomenological features) for the property of compounds not directly calculated via quantum mechanics [18].

Such computational searches can have their own limitations, working best for identifying a material with single target functionality but not when target ⬝⬝⬝⬝⬝⬝⬝⬝⬝⬝ are needed. Indeed, sometimes one wishes to find materials having simultaneously more than one target functionality. Compounds with simultaneous functionalities will be
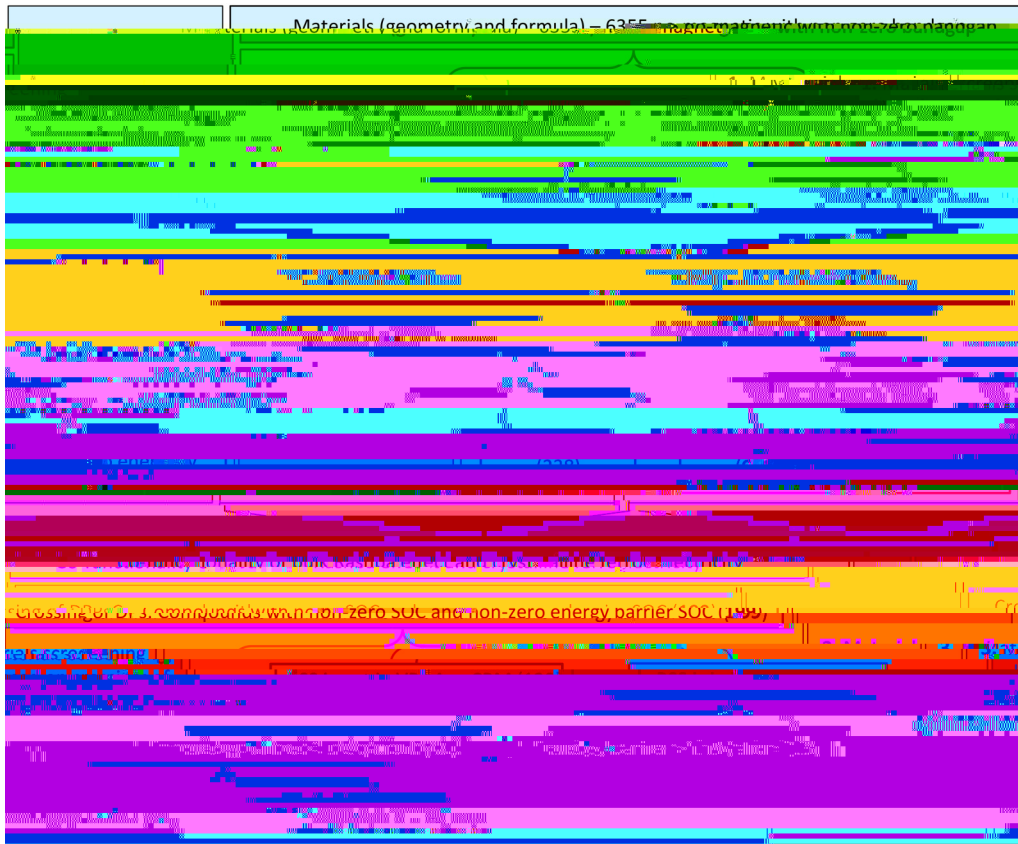
FIG. 3. Materials screening based on (line 1) the overlapping of design principles enabling single functionalities, (line 2) unique design principles for single functionalities, and (line 3) the crossing of the resulting lists. Additional design principles for the optimization of the cofunctionality for device applications are also included in step 3.

with helical spin texture perpendicular to the asymmetric potential, as represented in Fig. 1(c). The direction of this spin polarization depends on the electric dipole, i.e., opposite dipole direction leads to opposite spin-polarization direction.

Only few compounds have been reported thus far to have a large bulk Rashba coefficient, which is defined as the ratio between the spin splitting and the momentum offset , i.e., $\alpha = 2 \ / \ $ [Fig. 1(c)]. For this reason it has been thought that the Rashba effect is rather rare in nature [55]. Known examples include GeTe (3) [30,47], BiTeI ( ) [52,56], metallic PtBi$_2$ [57], the 2D organic-inorganic halide perovskite [ ] and [ ]C_6H_5

b4 and b5 guarantee the existence of the double well necessary in displacive ferroelectrics. In ferroelectrics, the transition state can also have multiple local motifs with nonzero local electric polarization that add up to zero (i.e., paraelectric structure) [65–67]. The theoretical modeling of this polymorphous structure requires the energy minimization with respect to the number of atoms used to define the unit cell [68,69].

(i.e., nonmagnetic), which results in 13 838 compounds, from which 6355 are gapped and nonmagnetic (i.e., band gap larger than 1 meV). As noted above [Fig. 2(a)], step 1 is the filtering

structures are traditionally assumed to have zero electric polarization, meaning that their space groups are CS. If the spontaneously electrically polarized structure has lower internal energy than the CS transition state, then an energy barrier separating opposite polarization states exists [DP b5 in Fig. 1(b)]. This barrier has to be surmountable to allow ferroelectric properties [DP b6 in Fig. 1(b)].

.   *f f* .   . *.. , *   .   . *.   *. *.,
, *   *f.   *. *   *   , * . , * *   *

. *( )* . Among the list of 230 crystalline space groups, as given by Table I, the CS ones have space-group numbers (arranged into a 3D Bravais lattice): triclinic (1), monoclinic (10–15), orthorhombic (47–74), tetragonal (83–88 and 123–142), rhombohedral (147, 148, and 162–167), hexagonal (175, 176, and 191–194), and cubic (200–206 and 221–230). For each nonpolar nonmagnetic insulator obtained from step 1, we determine all the symmetry groups that can be generated only by atomic displacements (from the original atomic positions) and classify them into the classes defined as centrosymmetric space groups (see Table I). The symmetry group identification in the displacive structures is performed using the symmetry detection algorithm of pymatgen [78] using atomic displace-

FIG. 5. Energy spectrum at the plane in the Brillouin zone of BrF_5. The color scale stands for the energy of the conduction bands with respect to the CBM. The energy minima along the Γ- symmetry line are indicated by the green points and $_\Gamma$. The band crossing (BC) along this path is also indicated by the white point. The spin texture for the polarization up and down ($_{Up}$ and $_{Down}$) is shown for the circular and rectangular inset.

spin splitting at the CBM of ≈ 30 meV with a Rashba parameter of 0.5 eV/Å (green square in Fig. 4). We identify two Rashba spin splittings along the Γ- symmetry line, which are indicated in the band structure as $_\Gamma$ and . Between these RSSs, there is a band crossing (BC) indicated by the white dot. As we will show, this BC has a helical spin texture.

2. , s, s

When this F atom is exactly equidistant from the two Br atoms, the BrF_5 space group is (see Table II) and the compound is centrosymmetric. This fact implies that the total electric polarization is zero (blue point in the double well represented in Fig. 4). The total energy of this transition state configuration is about 80 meV/atom higher than the ground states. As expected, since the electric polarization of the transition state (TS) is zero, its energy bands are spin degenerated, which is illustrated by the CBM in Fig. 4.

C. Confirmation of the reversal of spin texture when the FE polarization is flipped

Figure 5 shows the energy spectrum for the conduction band at the $_{xy}$ plane in the Brillouin zone of the FERSC BrF_5. The spin texture is shown for selected regions (indicated in green). The minimum energy for the Rashba spin splitting ($_\Gamma$ and) is indicated, as well as the band-crossing point. As shown in the circular region around the Γ point, the spin

texture of the configuration with polarization "Up" has opposite direction to the one for the structure with polarization "Down." This confirms the reversal spin texture expected in FERSCs.

V. CONCLUSIONS

We establish a standard inverse design approach for the search of cofunctionalities, which is based on causal physical models and not in numerical correlations as in machine learning approaches. This strategy is then applied to the special case of stable compounds that are simultaneously ferroelectric and bulk Rashba compounds. This inverse design approach is based on the causal physical design principles for enabling the Rashba effect, ferroelectricity, and cross-functionality. In a peanut schema, we first define common DPs and unique DPs for single functionalities. The compounds having the union of these DPs are then predicted to possess cofunctionality, when the specific cofunctionality does not require additional unique conditions. This inverse design approach reveals 52 previously synthesized compounds that were not realized to be FERSC having spin splitting at the band edges. In the list of predicted compounds, 24 FERSCs are in the most stable structure (on the convex hull). Some of the found compounds have giant spin splitting, e.g., BrF_5 (2_1), $TlIO_3$ (3), ZnI_2O_6 (2_1), $LaTaO_4$ (2_1), Tl_3S_3Sb (3), $Sn_2P_2Se_6$ ( ), and Bi_2SiO_5 (2_1) that have large Rashba spin splitting of 31, 57, 111, 40, 90, 67, and 76 meV, respectively.

The successful prediction of stable FERSCs with optimizing properties (e.g., Rashba bands at the band edges and small ferroelectric barrier) validates the proposed strategy. We hope that the theoretical prediction in this paper will be experimentally verified, which can open the way for future spintronic applications and the realization of devices based on the co-functionality of ferroelectricity and Rashba effect.

[1] A. Franceschetti and A. Zunger, The inverse band-structure problem of finding an atomic configuration with given electronic properties, Nature (London) **402**, 60 (1999).

[2] G. E. Eperon, T. Leijtens, K. A. Bush, R. Prasanna, T. Green, J. T.-W. Wang, D. P. McMeekin, G. Volonakis, R. L. Milot, R.

[24] G. Brunin, F. Ricci, V.-A. Ha, G.-M. Rignanese, and G. Hautier, Transparent conducting materials discovery using high-throughput computing, Npj Comput Mater **5**, 63 (2019).

[56] M. Sakano, J. Miyawaki, A. Chainani, Y. Takata, T. Sonobe, T. Shimojima, M. Oura, S. Shin, M. S. Bahramy, R. Arita, N. Nagaosa, H. Murakawa, Y. Kaneko, Y. Tokura, and K. Ishizaka, Three-dimensional bulk band dispersion in polar BiTeI with giant Rashba-type spin splitting, Phys. Rev. B **86**, 085204 (2012).

[57] Y. Feng, Q. Jiang, B. Feng, M. Yang, T. Xu, W. Liu, X. Yang, M. Arita, E. F. Schwier, K. Shimada, H. O. Jeschke, R. Thomale, Y. Shi, X. Wu, S. Xiao, S. Qiao, and S. He, Rashba-like spin splitting along three momentum directions in trigonal layered PtBi$_2$, Nat. Commun. **10**, 4765 (2019).

[58] Y. Zhai, S. Baniya, C. Zhang, J. Li, P. Haney, C.-X. Sheng, E. Ehrenfreund, and Z. V. Vardeny, Giant Rashba splitting in 2D organic-inorganic halide perovskites measured by transient spectroscopies, Sci. Adv. **3**, e1700704 (2017).

[59] S. Banik, P. K. Das, A. Bendounan, I. Vobornik, A. Arya, N. Beaulieu, J. Fujii, A. Thamizhavel, P. U. Sastry, A. K. Sinha, D. M. Phase, and S. K. Deb, Giant Rashba effect at the topological surface of PrGe revealing antiferromagnetic spintronics, Sci. Rep. **7**, 4120 (2017).

[60] M. E. Lines and A. M. Glass, *Principles and Applications of Ferroelectrics and Related Materials* (Oxford University, New York, 2001).

[61] W. Cochran, Crystal Stability and the Theory of Ferroelectricity, Phys. Rev. Lett. **3**, 412 (1959).

[62] G. Burns, Dirty displacive ferroelectrics, Phys. Rev. B **13**, 215 (1976).

[63] J. Valasek, Piezo-electric and allied phenomena in Rochelle salt, Phys. Rev. **17**, 475 (1921).

[64] P.-P. Shi, Y.-Y. Tang, P.-F. Li, W.-Q. Liao, Z.-X. Wang, Q. Ye, and R.-G. Xiong, Symmetry breaking in molecular ferroelectrics, Chem. Soc. Rev. **45**, 3811 (2016).

[65] M. Paściak, S. E. Boulfelfel, and S. Leoni, Polarized cluster dynamics at the paraelectric to ferroelectric phase transition in BaTiO$_3$, J. Phys. Chem. B **114**, 16465 (2010).

[66] M. B. Smith, K. Page, T. Siegrist, P. L. Redmond, E. C. Walter, R. Seshadri, L. E. Brus, and M. L. Steigerwald, Crystal structure and the paraelectric-to-ferroelectric phase transition of nanoscale BaTiO$_3$, J. Am. Chem. Soc. **130**, 6955 (2008).

[67] T. Nagai, Y. Mochizuki, H. Shirakuni, A. Nakano, F. Oba, I. Terasaki, and H. Taniguchi, Phase transition from weak ferroelectricity to incipient ferroelectricity in Li$_2$Sr(Nb$_{1-}$Ta$_{}$)O, Chem. Mater. **32**, 744 (2020).

[123] R. Gerardin, Preparation and identification of a new ternary compound, lithium beryllium antimonide (Li Be Sb), C. R. Acad. Sci. Ser. C **284**, 679 (1977).

[124] Ž. P. Čančarević, J. C. Schön, and M. Jansen, Possible existence of alkali metal orthocarbonates at high pressure, Chem. Eur. J. **13**, 7330 (2007).

[125] D. Zagorac, K. Doll, J. C. Schön, and M. Jansen, ꞏꞏ structure prediction for lead sulfide at standard and elevated pressures, Phys. Rev. B **84**, 045206 (2011).

[126] J.-Q. Dai and Z. Fang, Structural, electronic, and polarization properties of Bi_2ZnTiO_6 supercell from first-principles, J. Appl. Phys. **111**, 114101 (2012).

[127] S. Ju and G.-Y. Guo, First-principles study of crystal structure, electronic structure, and second-harmonic generation in a polar double perovskite Bi_2ZnTiO_6, J. Chem. Phys. **129**, 194704 (2008).

[128] S. Kashida, Electronic structure of Ag_2S, band calculation and photoelectron spectroscopy, Solid State Ionics **158**, 167 (2003).